Compact fermion to qubit mappings

Charles Derby [1,2,*] Joel Klassen [1,†] Johannes Bausch [1,3,‡] and Toby Cubitt [1,§]
[1]*Phasecraft Ltd, London, UK*
[2]*Department of Computer Science, University College London, Gower Street, London WC1E 6BT, UK*
[3]*Department of Applied Mathematics and Theoretical Physics, University of Cambridge, Trinity Lane, Cambridge CB2 1TN, UK*

(Received 16 July 2020; accepted 27 May 2021; published 8 July 2021)

Mappings between fermions and qubits are valuable constructions in physics. To date only a handful exist. In addition to revealing dualities between fermionic and spin systems, such mappings are indispensable in any quantum simulation of fermionic physics on quantum computers. The number of qubits required per fermionic mode, and the locality of mapped fermionic operators strongly impact the cost of such simulations. We present a fermion to qubit mapping that outperforms all previous local mappings in both the qubit to mode ratio and the locality of mapped operators. In addition to these practically useful features, the mapping bears an elegant relationship to the toric code, which we discuss. Finally, we consider the error mitigating properties of the mapping—which encodes fermionic states into the code space of a stabilizer code. Although there is an implicit tradeoff between low weight representations of local fermionic operators, and high distance code spaces, we argue that fermionic encodings with low-weight representations of local fermionic operators can still exhibit error mitigating properties which can serve a similar role to that played by high code distances. In particular, when undetectable errors correspond to "natural" fermionic noise. We illustrate this point explicitly both for this encoding and the Verstraete-Cirac encoding.

DOI: 10.1103/PhysRevB.104.035118

I. INTRODUCTION

One of the most striking features of fermions is the nonlocality of their state space. This nonlocality is necessitated by their antisymmetric exchange statistics—the phase of the wave function yielded by a fermion tracing a path past an even number of its counterparts differs from that yielded by a path past an odd number. However, causality is preserved by parity superselection [1], which forbids superpositions of even and odd fermion number, preventing the direct measurement of these phase differences.

A consequence of this nonlocality is that any representation of fermionic systems on collections of local quantum systems, such as qubits or distinguishable spins, must introduce nonlocal structure [2]. This is most readily seen in the Jordan-Wigner (JW) transform [3], which maps fermionic creation ($a_i^\dagger$) and annihilation (a_i) operators, which create and annihilate a fermion at mode i and satisfy the canonical anticommutation relations

$$\{a_i^\dagger, a_j\} = \delta_{ij}, \quad \{a_i^\dagger, a_j^\dagger\} = 0, \quad \{a_i, a_j\} = 0, \tag{1}$$

to stringlike Pauli operators

$$a_i^\dagger \to \tfrac{1}{2} Z_1 \ldots Z_{i-1}(X_i - iY_i). \tag{2}$$

Under this mapping even local observables conserving fermion parity, such as lattice hopping terms $(a_i^\dagger a_j + a_j^\dagger a_i)$, are mapped to strings of Pauli operators which may be as large as the size of the system.

The JW transform is an example of a mapping between fermions and qubits. Such mappings describe a correspondence between states of fermions and states of qubits, or, equivalently, between fermionic operators and multiqubit operators. They are restricted to fermionic systems with a discrete set of modes, since qubits possess finite dimensional Hilbert spaces, and are typically applied to fermionic lattice models. Many mappings are tailored to specific lattices.

A potential application where fermion to qubit mappings would be indispensable is the simulation of fermions by quantum computers. The accurate simulation of fermions has long posed a fundamental challenge to classical computers. Since the conception of quantum computers it has been understood that one of their primary applications would be in addressing this challenge, with substantial potential impact on a broad range of scientific disciplines.

Using a fermion to qubit mapping, a fermionic Hamiltonian may be mapped to a qubit Hamiltonian $H = \sum_i H_i$, with the terms H_i constituting tensor products of Pauli operators. A quantum computer can perform an effective simulation of the fermionic Hamiltonian by simulating time dynamics under H. The primary strategy to do this is via a Trotter expansion, which consists of dividing the time evolution unitary into a product of short evolutions generated by the terms H_i [4–6]. This is followed by a further decomposition of these short evolutions into sequences of quantum gates. However the greater the number of qubits on which these individual

*charlie@phasecraft.io
†joel@phasecraft.io
‡johannes@phasecraft.io
§toby@phasecraft.io

TABLE I. A comparison of existing local fermion encodings on an $L \times L$ lattice of fermionic modes. The compact encoding presented in this work is given in the three rightmost columns. Max weight Coulomb and max weight hopping denote the maximum Pauli weights of the mapped Coulomb ($a_i^\dagger a_i a_j^\dagger a_j$) and nearest neighbor hopping ($a_i^\dagger a_j + a_j^\dagger a_i$) terms, respectively. Encoded fermionic space denotes whether the full or even fermionic fock space is represented. Graph geometry denotes the hopping interaction geometry which the mapping is tailored to.

Mapping	[13]	[10,11]	[15]	[12]	[14]	even face number	majority even faces	majority odd faces
Qubit Number	$2L(L-1)$	$2L^2$	$2L(L-1)$	$2L^2-L$	$3L^2$	$1.5L^2-L$	$1.5L^2-L-1$	$1.5L^2-L+1$
Qubit to Mode Ratio	$2-\frac{2}{L}$	2	$2-\frac{2}{L}$	$2-\frac{1}{L}$	3	$1.5-\frac{2}{L}$	$1.5-\frac{2}{L}-\frac{1}{2L^2}$	$1.5-\frac{2}{L}+\frac{1}{2L^2}$
Max Weight Hopping	6	4	4	5	4	3	3	3
Max Weight Coulomb	8	2	6	6	6	2	2	2
Encoded Fermionic Space	Even	Full	Even	Full	Even	Full	Even	Full Plus Qubit
Graph Geometry	General	General	Square Lattice	Square Lattice	General	Square Lattice	Square Lattice	Square Lattice

Hamiltonian terms H_i act—i.e., the Pauli weight—the more costly the circuit decomposition [7,8]. Similar considerations also inform the performance of other quantum algorithms, such as VQE [9]. Thus, there has emerged a practical need to design fermion to qubit mappings which minimize the Pauli weight of commonplace fermionic operators. In particular those fermionic interactions which couple nearby fermionic modes—i.e., geometrically local operators—which feature prominently in physically realistic systems.

The JW transform performs poorly in this respect because all of the requisite fermionic nonlocality is manifest in the observables, as opposed to the states—the fermionic Fock states map directly to seperable binary states. One may instead design a mapping which encodes the nonlocality in the states, by mapping fermionic states into a highly entangled subspace of the multiqubit system. In this way one can retrieve low weight qubit representations of geometrically local fermionic operators. We refer to such mappings as *local fermionic encodings*.

There currently exist a handful of local fermionic encodings [10–15]. A comparison of these encodings is given in Table I. Two terms which are ubiquitous in fermionic Hamiltonians are lattice hopping, and Coulomb interactions. The minimum upper bounds on the Pauli weights of these terms under any of these encodings is 4 and 2, respectively. Furthermore, all of these encodings employ approximately 2 or more qubits per fermionic mode.

In Sec. II of this work we present a local fermionic encoding—which we call the compact encoding—that not only outperforms all existing local encodings in terms of Pauli weight, yielding for instance max weight 3 hopping terms, but also employs fewer than 1.5 qubits per mode. We expect these features to find significant use in near-term quantum computing applications, where resources are limited. The mapping can be thought of as a modified toric code [16,17] that condenses local pairs of particle excitations, yielding a low energy subspace which corresponds to a fermionic Hilbert space. For clarity we focus in this work on the square lattice; however, the design scheme of the encoding may also be applied to other interaction graphs, yielding similar cost benefits. In Appendix B we illustrate how the scheme may be applied to a hexagonal lattice.

All local encodings map fermionic states into a subspace of a multiqubit Hilbert space via the formalism of stabilizer codes, by defining a set of mutually commuting Pauli operators (stabilizers) for which the subspace constitutes a common $+1$ eigenspace. Stabilizer codes are commonly employed in the detection and/or correction of physical qubit errors. It is therefore natural to consider to what extent the existing local fermionic encodings can correct or detect physical qubit errors. However, good error correcting/detecting codes must have high weight logical operators, so that the code distance is not small. Thus, error correction/detection is seemingly at odds with the goal of low-weight logical fermionic operations. For example, there exist two local fermionic encodings [14,15] that are also error correcting codes. Although both yield weight 4 hopping terms, the coulomb terms are weight 6. In contrast the compact encoding yields weight 2 coulomb terms.

In Sec. III we argue that, despite the apparent conflict between low-weight fermionic operators and error correction/detection, there can exist valuable error mitigating properties of fermionic encodings that do *not* need to be sacrificed in the pursuit of low-weight fermionic operators, and that the compact encoding exhibits such properties. In particular, in the context of fermionic simulation of natural systems, one might tolerate—or even desire—some noise in the physical qubits, provided that this noise translates into "natural" fermionic noise in the simulated fermionic system. The notion that hardware level noise may be translated into simulated noise is explored in generality in Ref. [18]—we consider how this reasoning applies in the specific context of fermionic encodings and in particular to the compact encoding and the Verstraete-Cirac (VC) encoding. We catalog all weight-1 errors that are correctable/detectable in the compact encoding and show that the remaining weight-1 errors may be understood as local fermionic phase noise in the code space.

Such fermionic phase noise appears naturally in fermionic systems coupled to a bosonic bath, such as phonons in a lattice. We additionally show how these error mitigating features may be employed in a simulated time evolution algorithm.

II. THE COMPACT ENCODING

There are two design strategies that all existing local fermionic encodings employ. One strategy, employed by encodings presented in Refs. [10–12], leverages the Jordan-Wigner transform, and defines stabilizers that "cancel out" sections of the long strings, discarding a portion of the fermionic modes in the process.

The second strategy, employed by the encodings presented in Refs. [13–15], as well as the compact encoding presented here, focuses instead on finding a set of low weight Pauli operators which reproduce all of the local (anti)-commutation relations of the fermionic "edge" (E_{jk}) and "vertex" (V_j) operators—which are most concisely defined in terms of Majorana operators $\gamma_j := a_j + a_j^\dagger$ and $\overline{\gamma}_j := (a_j - a_j^\dagger)/i$:

$$E_{jk} := -i\gamma_j\gamma_k, \quad V_j =: -i\gamma_j\overline{\gamma}_j. \tag{3}$$

These operators are Hermitian, traceless, self inverse and satisfy $E_{jk} = -E_{kj}$. Pairs of such operators anticommute if and only if they share an index, and encodings of this second kind aim to reproduce these local (anti)-commutation relations. More precisely,

$$\{E_{jk}, V_j\} = 0, \quad \{E_{ij}, E_{jk}\} = 0, \tag{4}$$

and for all $i \neq j \neq m \neq n$,

$$[V_i, V_j] = 0, \quad [E_{ij}, V_m] = 0, \quad [E_{ij}, E_{mn}] = 0. \tag{5}$$

All even fermionic operators (i.e., even products of creation and annihilation operators and sums thereof) can be expressed in terms of edge and vertex operators [13]. Furthermore, all parity preserving operators are even fermionic operators and so in accordance with parity superselection all physical fermionic observables are even fermionic operators.

Associating Pauli operators to each edge and vertex operator such that the above conditions are satisfied almost completely defines a mapping from the even fermionic operators to qubit operators. However there exists an additional nonlocal relation: the product of any loop of edge operators must equal the identity. More precisely,

$$i^{(|p|-1)} \prod_{i=1}^{(|p|-1)} E_{p_i p_{i+1}} = \mathbb{1} \tag{6}$$

for a cyclic sequence of sites $p = \{p_1, p_2, \ldots, p_{|p|} = p_1\}$.

Given a mapping from edge operators to Pauli operators, the expression on the left hand side of Eq. (6) also in general maps to a Pauli operator. However, by restricting the mapped fermionic states to the common $+1$ eigenspace of these Pauli operators (i.e., taking them to be the stabilizers), Eq. (6) becomes satisfied in that subspace.

For all prior encodings which have employed this second strategy, the stabilizers additionally generate the total fermion parity operator $\prod_i V_i$, fixing its value to $+1$, so that the mappings only admit representations of even fermionic states. The mapping given in this work is the first employing this design strategy that can avoid this side-effect. In this case one may represent states violating parity superselection, and so the full fermionic algebra admits a representation. This additional structure is completely specified by mapping a single Majorana operator to a qubit operator, satisfying appropriate (anti)-commutation relations.

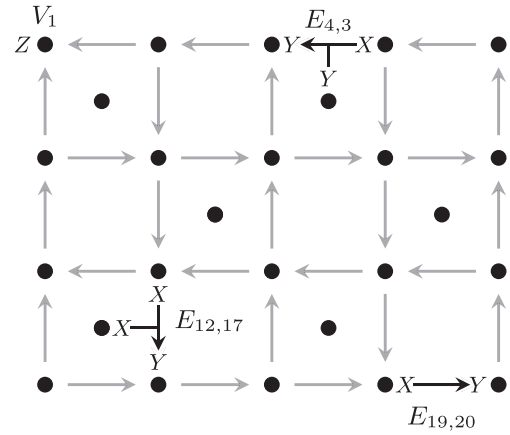

FIG. 1. Qubit assignment, edge orientation, and examples of mapped edge and vertex operators for a 4×5 square lattice. Vertices are numbered left to right, top to bottom.

We now proceed with a complete description of the compact encoding (See Appendix C for proof of correctness of the encoding). It suffices to define mappings from edge and vertex operators to qubit operators. Consider a square lattice of fermionic sites at the vertices. Label the faces of the lattice even and odd in a checker-board pattern. For each fermionic site j associate a "vertex" qubit indexed by j. Associate a "face" qubit to the odd faces. Assign an orientation to the edges of the lattice so that they circulate around the even faces clockwise or counterclockwise, alternating on every row of faces. This is illustrated in Fig. 1. We refer to the vertex qubits as "primary" qubits, and the face qubits as "auxiliary" qubits.

Here and throughout we denote mapped operators with a tilde overscript. Let $f(i, j)$ index the unique odd face adjacent to edge (i, j). For every edge (i, j), with i pointing to j, define the following mapped edge operators:[1]

$$\tilde{E}_{ij} := \begin{cases} X_i Y_j X_{f(i,j)} & (i,j) \text{ oriented down}, \\ -X_i Y_j X_{f(i,j)} & (i,j) \text{ oriented up}, \\ X_i Y_j Y_{f(i,j)} & (i,j) \text{ horizontal.}, \end{cases} \tag{7}$$

$$\tilde{E}_{ji} := -\tilde{E}_{ij}. \tag{8}$$

For those edges on the boundary which are not adjacent to an odd face, omit the Pauli operator that would otherwise be acting on a face qubit. For every vertex j define the mapped vertex operators

$$\tilde{V}_j := Z_j. \tag{9}$$

This specifies all mapped vertex and edge operators and is illustrated in Fig. 1.

[1]The difference in sign introduce between the vertical up and down orientations is included to ensure that cycles around odd faces are equal to $\mathbb{1}$ and not $-\mathbb{1}$.

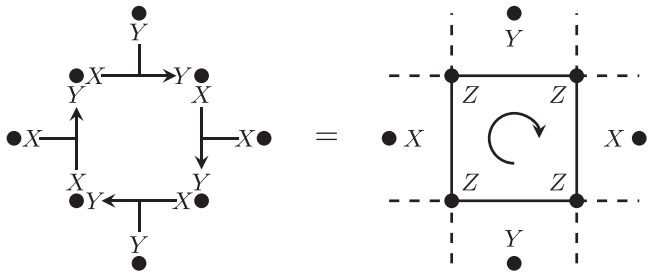

FIG. 2. Nontrivial stabilizer of the encoding.

This mapping satisfies the local (anti-)commutation relations Eqs. (4) and (5). The intuition is that a directed edge has an X on the tail and a Y on the head. Whenever the head of one edge touches the tail of another the edge operators anticommute, while if two edges touch head to head or tail to tail they commute. By adding a qubit at some faces, and choosing an appropriate orientation for the edges, one can enforce the additional necessary anticommutation relations at the face qubits.

Given a lattice with M fermionic modes, this encoding uses fewer than $1.5M$ qubits. Furthermore this construction yields hopping and Coulomb terms with Pauli weight at most 3. The reason that the Pauli weights and qubit numbers are so low is that the face qubits are used extremely efficiently, each one enforcing anticommutation relations at four bounding corners.

To satisfy Eq. (6) one must project into the common $+1$ eigenspace of all loops of edge operators. In the case of a planar graph the loops around faces form a minimal generating set. The stabilizers associated with even faces are nontrivial and illustrated in Fig. 2, while the stabilizers associated with odd faces are equal to $\mathbb{1}$. Therefore, the number of independent constraints, dividing the Hilbert space in two, is given by the number of even faces. By a simple counting argument the dimension of the subspace to which fermionic states are mapped is thus given by

$$\text{subspace dimension} = 2^{\mathrm{M+OF-EF}}, \tag{10}$$

where M is the number of fermionic modes, OF is the number of odd faces, and EF is the number of even faces.

There are three distinct cases for which the subspace dimension differs:

(I) There are an even number of faces, and so an equal number of even and odd faces.

(II) There is one more even face than odd face.

(III) There is one more odd face than even face.

The reader may wish to examine sublattices in Fig. 1 to develop an intuition for these cases.

In case (I) the encoding represents the full fermionic Fock space $\mathbb{F}$, with dimension 2^{M}. Therefore, single Majorana operators also admit a representation. It suffices to specify one Majorana, and all others may be constructed using edge and vertex operators. A Majorana operator γ_j must anticommute with all edges incident on site j as well as the vertex operator V_j. Any corner vertex j which bounds an odd face must either have arrows pointing into it or pointing away from it. If the arrows point into (away from) the corner, then the mapped Majorana is $\tilde{\gamma}_j = X_j$ (Y_j). There are two possible choices of corners. The choice is arbitrary, but once a corner is chosen then the equivalent operator at the remaining corner corresponds to a Majorana hole operator $h_i := \gamma_i \prod_j V_j$.

In case (II) the dimension of the subspace is $2^{\mathrm{M}-1}$, which is half of the full fermionic Fock space. Furthermore, up to multiplication by stabilizers, $\prod_i \tilde{V}_i = \mathbb{1}$. Thus, this encoding represents the even fermionic Fock space. This is evidenced by the fact that there are no corner vertices bounding odd faces on which to define a Majorana operator.

Finally, in case (III) the dimension of the subspace is $2^{\mathrm{M}+1}$, i.e., the full fermionic Fock space plus an additional "logical" qubit degree of freedom: $\mathbb{F} \otimes \mathbb{C}^2$. In this case there are four corner vertices on which to define a Majorana operator. These four Majoranas can be thought of as four distinct species A_i, B_i, C_i, and D_i, each introduced at a different corner and translated by edge operators to site i. Pairwise annihilation of differing species of Majorana yield three distinct vacua: ϵ_1, ϵ_2, ϵ_3. Identifying one species of Majorana (in this case A) to act as the canonical Majorana operator on the fermionic system and identity on the logical qubit, the other three species become identified with majorana hole operators multiplied by logical Pauli operators on the logical qubit.

$$A_i = \tilde{\gamma}_i \otimes \mathbb{I}, \tag{11}$$

$$B_i = \tilde{h}_i \otimes \tilde{X}, \quad C_i = \tilde{h}_i \otimes \tilde{Y}, \quad D_i = \tilde{h}_i \otimes \tilde{Z}. \tag{12}$$

The vacua are thus identified with applying logical Pauli operators on the logical qubit:

$$\epsilon_1 = \tilde{X}, \quad \epsilon_2 = \tilde{Y}, \quad \epsilon_3 = \tilde{Z}. \tag{13}$$

These logical Pauli operators are mapped to multiqubit Pauli operators which span the length of the system (see Appendix A for more details), thus the logical qubit is topologically protected. This is highly suggestive of a connection to the toric code.

Indeed the stabilizers of the encoding presented here are tensor products of toric code star (Π_S) and plaquette (Π_P) operators on the face qubits (up to local rotations) and four qubit Z parity checks on the vertex qubits. This is illustrated in Fig. 3.

The toric code Hamiltonian

$$H_{\mathrm{toric}} = -\sum \Pi_S - \sum \Pi_P \tag{14}$$

has localized electric (e) and magnetic (m) excitations, corresponding to energy contributions from Π_S and Π_P terms. These excitations exhibit fermionic mutual statistics and bosonic self statistics. Consequently a composite of e and m excitations exhibits fermionic self statistics. The addition of the four qubit Z parity operators yields a modified Hamiltonian,

$$H_{\mathrm{map}} = -\sum \Pi_S \otimes Z_s - \sum \Pi_p \otimes Z_p, \tag{15}$$

for which specific localized pairings of e and m particles no longer cause an energy penalty. More concretely, any path of edge operators $E_{ij} = -i\gamma_i\gamma_j$ corresponds to the creation of a pair of Majoranas at either end of the path. Each of these Majoranas give rise to bound pairs of e and m particles in H_{toric} which have no energy penalty in H_{map} and exhibit fermionic exchange statistics. This is illustrated in Fig. 4.

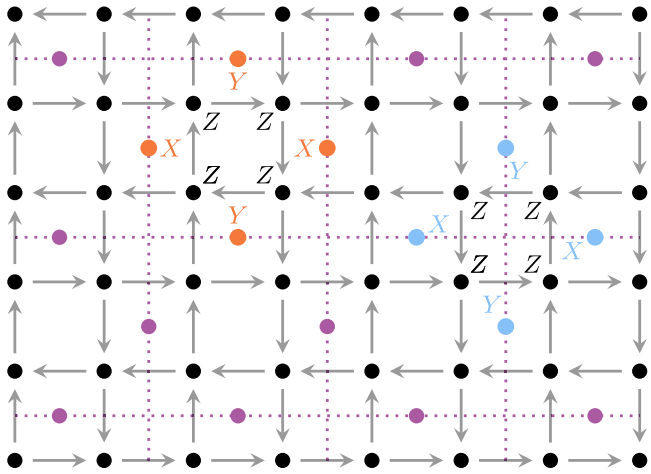

FIG. 3. The toric code (dotted purple) embedded in the compact encoding. Each stabilizer is a tensor product of either a plaquette Π_p (red) or star Π_s (blue) operator, with a four qubit Z parity operator (black).

In this sense the compact encoding leverages the topological order of the toric code to generate nonlocal exchange statistics. Similar connections appear in other fermionic encodings [10,13,15] but not as explicitly.

III. ERROR MITIGATING PROPERTIES

The compact encoding represents fermions in a stabilizer code space and thus can be analyzed within the framework of quantum error correction. Operators that commute with elements of the stabilizer group are logical operators and preserve the code space. Operators that do not commute take states out of the code space and can thus be detected by stabilizer measurements—these operators are called detectable. If the stabilizer measurements yield a unique signature, then the operators are called correctable. For the purposes of reducing error rates it is preferable to engineer a code to detect or correct as many error operators as possible. We begin by cataloguing all weight-1 qubit errors that are undetectable in the compact encoding. Our analysis here is motivated by the assumption that weight-1 Pauli noise dominates in the given noise model. This is consistent with the most commonly studied qubit noise model, iid depolarising noise, amongst others.

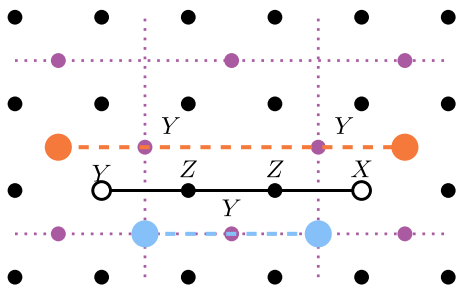

FIG. 4. A pair of Majorana particles, generated by a string of edge operators (black) in the compact encoding correspond to localized pairs of e (blue) and m (red) particles in the toric code.

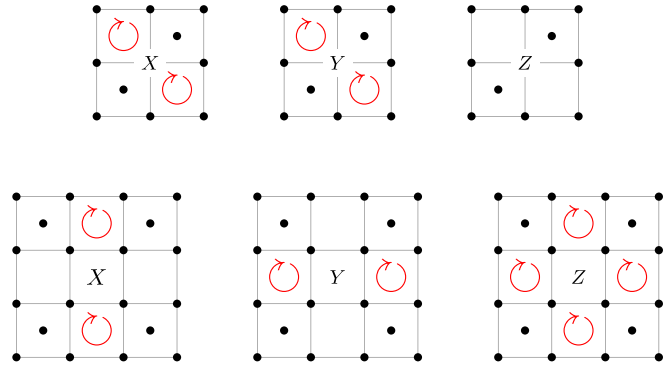

FIG. 5. Graphical representation of the syndromes of single qubit errors on the compact encoding on vertex qubits (upper) and face qubits (lower). The red circlular arrows represent the loop stabilizers that anticommute with the given error. Z on a vertex qubit has no syndrome as it is a logical operator. For boundary cases where a highlighted stabilizer does not exist, it is omitted from the syndrome. Note that errors on vertex qubits can occur in contexts where the odd and even faces are inverted from how they are illustrated here. In this case the syndrome is similarly inverted.

Theorem 1. In the compact encoding for square lattices, the only nontrivial, undetectable, Pauli weight-1 errors are:

(1) Z operators on primary qubits, which map to mode-weight-1 fermionic phase errors $Z_j \mapsto -\mathrm{i}\gamma_j\overline{\gamma}_j$.

(2) In the case where the full fermionic space is encoded, X or Y errors on those corners adjacent only to an odd face, which map to single Majorana or Majorana hole operators, depending on the choice of convention.[2]

Proof. There can be X, Y, or Z errors, either on the lattice face qubits (auxiliary qubits), or the vertices (primary qubits). We address them separately.

a. Auxiliary Qubits. By inspection of the syndromes of single qubit errors shown in Fig. 5, it is evident that Pauli weight 1 errors on face qubits always have a syndrome and are thus detectable.

b. Primary Qubits. Any Z errors on vertex qubits are undetectable as they have no syndrome; they correspond to fermionic phase errors. However, X and Y errors on vertex qubits *are* detectable, as they induce syndromes on two diagonally offset loop stabilizers. However, there may be corners of the lattice which are not touching a stabilizer (i.e., a corner which only touches an odd face). X or Y errors on those vertex qubits correpond to single Majorana or Majorana hole operators. These are parity switching errors, so are not possible if only the even fermionic subspace is encoded. ■

To summarize, all weight-1 qubit errors fall into one of three categories: detectable errors; errors that correspond to phase noise on a single mode; and a small number of errors that correspond to Majorana operators on a single mode. We note that the VC encoding has exactly these properties as well.

[2]For example, $X_i \mapsto \gamma_i$, $Y_i \mapsto \overline{\gamma}_i$ or $X_i = \gamma_i \prod_j (-i\gamma_j\overline{\gamma}_j)$, $Y_i \mapsto \overline{\gamma}_i \prod_j (-i\gamma_j\overline{\gamma}_j)$. For a fixed fermionic parity, the operator $\prod_j (-i\gamma_j\overline{\gamma}_j)$ is a good quantum number equal to ± 1, and so fermionic hole operators can be thought of as mode-weight-1 fermionic operators.

This is originally discussed in Ref [15]—although there exists a Majorana error occurring on the first data qubit which that work overlooks—and thus many of the following considerations hold equally well for the VC encoding.

Although the Majorana errors can only occur on very few sites, they can take a fermionic state into one which violates parity superselection. In Sec. III A we present some alternative techniques for avoiding or detecting these errors.

Ignoring for the moment the Majorana errors we turn our attention to the on-site phase errors $-\mathrm{i}\gamma_j\overline{\gamma}_j$ associated with Z operators on the primary qubits of the compact encoding as well as the VC encoding. A common fermionic lattice model is one in which lattice sites correspond to atomic positions. These atomic positions are often considered to be fixed. However, one may consider the possibility of phonons in the lattice of atoms, and how these phonons couple to the electrons as a source of noise. To first order, this coupling is dominated by low energy acoustical modes [19,20], with interaction Hamiltonian

$$H_{\mathrm{int}} = \frac{1}{V}\sum_{\mathbf{k},\sigma}\sum_{\mathbf{q}} g_{\mathbf{q}} a^{\dagger}_{\mathbf{k}+\mathbf{q},\sigma} a_{\mathbf{k},\sigma}(b_{\mathbf{q}} + b^{\dagger}_{-\mathbf{q}}), \tag{16}$$

where $a^{(\dagger)}_{\mathbf{k}}$ and $b^{(\dagger)}_{\mathbf{k}}$ are, respectively, the annihilation and creation operators for fermions and phonons with momentum $\mathbf{k}$.

For a thermal bosonic bath, the effective noise model of this interaction on the fermionic system is spontaneous hopping of fermions into different momentum modes. In the position basis this translates into dephasing noise [21], since motion in momentum space corresponds to phase shifts in position space. The fermionic dephasing operator is

$$(1 - 2N_j) = -\mathrm{i}\gamma_j\overline{\gamma}_j. \tag{17}$$

We present a more thorough account of the derivation of this noise model in Appendix D.

Thus, we see that, given an appropriate choice of particle basis to which the fermionic modes of a lattice model are chosen to correspond, every undetectable error in the compact encoding and the VC encoding—excluding the Majorana errors—may be interpreted as local and natural physical noise in the simulated fermionic system. In cases where incorporating the effect of natural thermal noise into the simulation is acceptable (or even desirable), then instead of detecting or correcting such errors, one might be satisfied with accepting such errors in the simulation. We discuss the mechanics of this in Sec. III B.

Finally, we note that if one chooses to accept Pauli Z errors on primary qubits, then this generates an equivalence relation between X and Y errors on primary qubits, such that they become effectively correctable. More specifically, the signatures of an X and Y error on a primary qubit are identical. Thus, applying a random X or Y correction in response to such a syndrome will either successfully remove the error or introduce a Z error, which maps onto natural fermionic phase noise. This, together with the fact that all single qubit Pauli errors on auxiliary qubits are correctable in both the VC and compact encodings, implies that active error correction could in principle be deployed for all single qubit errors, provided one is willing to accept additional phase noise in the simulated fermionic system. All of this is of course predicated on the assumption that one avoids the Majorana errors, which is addressed in the next section.

A. Avoiding Majorana errors

Depending on the choice of orientation, lattice shape and convention, an X or Y error on the compact encoding at the corners of the lattice may be undetectable and map to a single Majorana error γ_i or $\overline{\gamma}_i$. These Majorana errors can be quite serious—if they occur coherently, then they may yield encoded states that correspond to unnatural fermionic states which violate parity superselection.

Of course, any error that breaks parity superselection, such as single Majoranas, can be detected by simply measuring the parity of the fermionic system as a stabilizer. This parity stabilizer is given by the product of vertex operators at every fermionic site, which in the case of the compact encoding (and the VC encoding) corresponds to the product of Z operators on every primary vertex qubit. However, if one is performing nondestructive and coherent stabilizer measurements, or is interested in measuring observables that do not commute with the vertex operators, then such a stabilizer can be very costly to measure coherently.

Majorana errors appear in the VC encoding in a similar fashion to the compact encoding, and we make a brief comment on these to start, before proceeding with strategies for mitigating these errors in the compact encoding. The principle behind the VC encoding is that the fermionic system is represented using the JW transform; however, the long strings of Z operators are avoided by interleaving auxiliary fermionic modes in the linear ordering of the JW transform, and defining stabilizers to be those interactions between auxiliary modes which are adjacent in the desired lattice geometry but not in the linear ordering. These stabilizers may be used to cancel the strings of Z operators that would otherwise appear in the interactions between the primary modes. Under the standard interleaving of the modes—alternating primary and auxiliary—an X or Y operator on the first primary mode is undetectable and acts as a majorana operator. We note that simply exchanging the ordering of the first primary and auxiliary modes—while leaving the order of the remaining modes unchanged—solves this problem (making the Majorana operator weight 2) at no cost to the performance of the VC encoding.

Returning to the compact encoding, we note that an even $\times$ even lattice can avoid parity switching errors altogether by choosing the appropriate checkerboard pattern of the auxiliary qubits such that none are placed in corner faces, permitting only the representation of parity-preserving fermionic operators. Even $\times$ odd and odd $\times$ odd lattices always have auxiliary qubits in two corners and so will always permit Majorana errors. In a similar fashion to the VC encoding, modifying the structure of the compact encoding also allows one to avoid these errors.

If the two corner fermionic sites adjacent to the odd faces are removed as shown in Fig. 6, then the parity switching errors correspond to Pauli weight-2 errors—i.e., the single Majorana or hole operator—has a weight-2 qubit representation. One can preserve most of the structure of the corner, by introducing a new diagonal edge operator connecting those

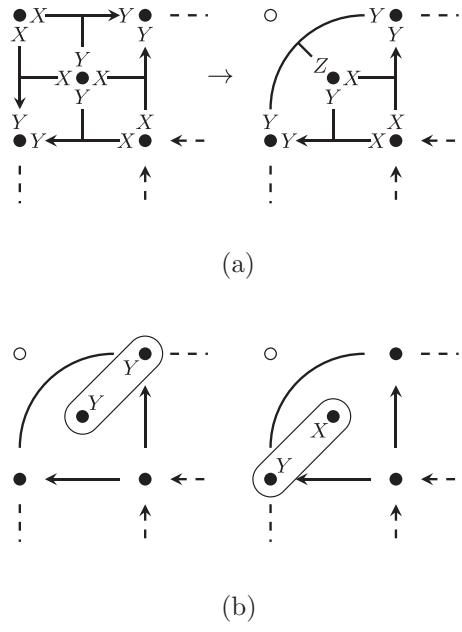

FIG. 6. Lattice modification to create weight-2 single Majorana/hole operators. (a) The change in edge operators, (b) the Majorana/hole operators on the new corner sites. For a corner face where the arrows are all pointing in the other direction, the action of the new edge operator and the new Majorana operators on the vertex qubits will be X.

vertex qubits which had previously been connected to the removed site. To ensure the correct anticommutation relations, this new edge operator acts with a Z on the face qubit and will act with the same Pauli operator on its incident vertex qubits as the two edge operators bounding the odd face (see Fig. 6). The cycle operator formed by these three edge operators is the identity, provided the correct sign convention is chosen for the diagonal edge.

Single Majorana (or Majorana hole) operators may be added on either of the sites which were previously adjacent to the removed corner site, by applying a weight-2 Pauli operator on the corresponding vertex qubit and on the face qubit. Note that these operators anticommute with all incident edge operators and the vertex operator on that site.

A final way to modify the lattice to avoid undetectable Majorana errors is to introduce periodic boundary conditions. This yields a uniform periodic lattice if and only if the number of faces (which equals the number of lattice vertices) is even in both directions. Note that in this case the code space dimension is 2^{M-1}.[3] Given such a torus, and by inspection of the error syndromes in Fig. 5, the following claim is immediately evident.

Proposition 1. On a torus with an even face count $\geqslant 4$ in both directions, any two weight-1 Pauli errors are either completely detectable; a combination of at most one detectable error and one fermionic phase noise term; or two weight-1 fermionic phase noise terms.

Proof. In the case of periodic boundary conditions, the only single-error syndromes are those illustrated in Fig. 5, with none being truncated at the boundaries. The only pairing of error syndromes in Fig. 5 that cancel are an X and Y error on the same vertex qubit, which simply corresponds to a Z error on a vertex qubit, i.e., fermionic phase noise. ■

For a sufficiently large lattice with periodic boundary conditions, all weight-2 errors either correspond to natural simulated noise, or are detectable. Clearly then, in the absence of periodic boundaries, undetectable weight-2 errors that do not correspond to phase noise must only appear on the boundary of the lattice.

B. Error mitigation in Hamiltonian simulation

As we have seen so far, several types of Pauli weight 1 errors are detectable within the compact encoding. This fact can be exploited for Hamiltonian simulation to allow for a higher effective Pauli noise rate, by postselecting on runs without stabilizer violations, either during or at the end of the computation. More specifically, let us assume we are given a fermionic Hamiltonian H_F built from fermionic creation and annihilation operators, and we can decompose $H_F = \sum_j H_j$ such that the support of the H_j is disjoint. We wish to implement a time dynamics simulation of the system via Trotterization [4]; for instance, for a small time-step δ, we approximate

$$e^{-iH_F T} \simeq \prod_{n=0}^{T/\delta} \prod_j e^{-iH_j \delta} + O(\delta). \tag{18}$$

The simulation thus progresses by sequentially applying unitary operations generated by the H_j; as each of them comprises only operators that commute with the stabilizers it is clear that any single stabilizer violation emerging from an error midway through the simulation will remain detectable after the simulation finishes. However, in addition to undetectable errors, there now is also the possibility of having the same stabilizer-violating error on the same site, twice, such that those errors exactly cancel; or, alternatively, a combination of multiple errors such that the syndrome patterns in Fig. 5 line up and cancel exactly.

IV. DISCUSSION

The compact encoding constitutes a significant improvement on both the mode-to-qubit ratio and the Pauli weights of local operators. For near-term quantum computing hardware, such gains are essential. See Ref. [8] for an example of how this encoding can yield significant improvements in quantum simulation algorithms. The design principles outlined for this encoding can also be applied to other lattice types. In forthcoming work we consider how the compact encoding can be applied to various planar and 3D lattices, with similar improvements on operators weights and qubit to mode ratios.

The error mitigating properties of this encoding are also particularly relevant for near-term quantum algorithms with no active error correction or fault tolerance. Since fermionic

[3]To see this note that two additional nontrivial stabilizers are introduced corresponding to topological cycles, but now the set of nontrivial face stabilizers is overcomplete, since the product of all nontrivial face cycles is identity.

encodings are indispensable for fermionic simulation, they constitute a significant fixed overhead in representing any fermionic systems on NISQ devices. One may not be able to afford any additional overhead for supplementary error detection. In this context the time scale of any coherent quantum evolution would have to be upper bounded to ensure that the probability of an error is $\ll 1$. Individual runs might then be post-selected based on whether errors are detected. Even if one does have fault tolerance, mitigating a large fraction of errors already one level above the error-correcting code would allow a reduction in overhead.

In our discussion of the relationship between the compact encoding and the toric code, we illustrate how the encoding condenses specific particle excitations of the toric code into the code space of the compact encoding. We note that similar strategies might be applicable to the particle excitations of other codes.

ACKNOWLEDGMENT

We thank Laura Clinton, Raul Santos, and Tom Scruby for their helpful discussions.

APPENDIX A: DETAILS OF LOGICAL QUBIT OPERATORS IN CASE III

As discussed in the main text, in case (III) the encoded subspace consists of the full fermionic Fock space plus an additional logical qubit degree of freedom ($\mathbb{F} \otimes \mathbb{C}^2$) and the square lattice has four corners from each of which either all incident edges point into or away. Applying an X Pauli operator at a corner where edges point away (and Y where edges pointing into) must correspond to applying an encoded Majorana or hole operator ($h_i := \gamma_i \prod_k V_k$)—as these are the only fermionic operators satisfying the resulting (anti-)commutation relations at that site—along with potentially some additional action on the logical qubit space. We define the four operators A_i, B_i, C_i, and D_i, each corresponding to a distinct corner, as the application of an X (or Y) at that corner followed by the application of a sequence of edge operators from the corner to site i. These operators satisfy the following (anti-)commutation relations $\forall i \neq j$ and $\forall M \neq M' \in \{A, B, C, D\}$:

$$\{M_i, M_j\} = [M_i, M'_j] = \{M_i, M'_i\} = 0. \tag{A1}$$

An assignment of Majorana, hole, and Pauli operators to these M which satisfy these commutation relations is

$$A_i = \tilde{\gamma}_i \otimes \mathbb{I}, \tag{A2}$$

$$B_i = \tilde{h}_i \otimes \tilde{X}, \quad C_i = \tilde{h}_i \otimes \tilde{Y}, \quad D_i = \tilde{h}_i \otimes \tilde{Z}. \tag{A3}$$

One can retrieve the isolated logical Pauli operators by taking the product of select pairs:

$$C_i D_i = i\mathbb{I} \otimes \tilde{X}, \tag{A4}$$

$$D_i B_i = i\mathbb{I} \otimes \tilde{Y}, \tag{A5}$$

$$B_i C_i = i\mathbb{I} \otimes \tilde{Z}. \tag{A6}$$

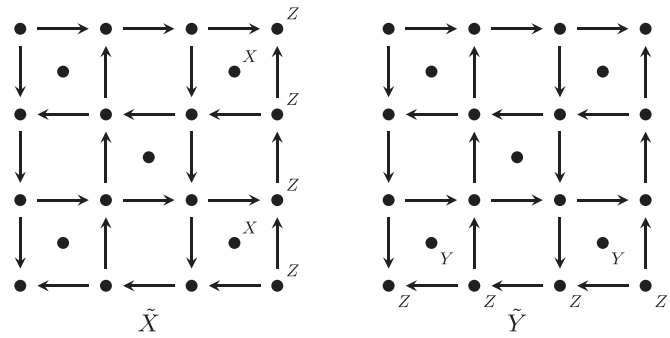

FIG. 7. The logical X and Y operators on the extra logical qubit in case (III).

Such products correspond to string-like operations extending the length of the lattice, from one corner to another. Examples of these operators are illustrated in Fig. 7. Note that if one treats one of these operators as a stabilizer, then one restricts to the full fermionic code space without an extra logical qubit. In this case, as one should expect, there are only two corners in which to inject a Majorana, since injecting a Majorana at either of the other two corners would anticommute with the chosen stabilizer. These two corners correspond to the Majorana and its hole counterpart, as in case (I) where there are only two odd corners.

APPENDIX B: HEXAGONAL LATTICE MAPPING

Hexagonal lattices admit a similar construction to that described in the main text for square lattices. Again we follow the scheme of orienting the edges, introducing ansatz edge operators with an X at the tail and a Y at the head, and then introducing interactions on face qubits to satisfy the anticommutation relations.

In the hexagonal lattice every edge, except for the bottom edge of every face, is oriented clockwise on even columns of faces and counterclockwise on odd columns, as illustrated in Fig. 8. This ensures that heads touch tails for all edges except for the bottom edge of every hexagon. A qubit is introduced at every face.

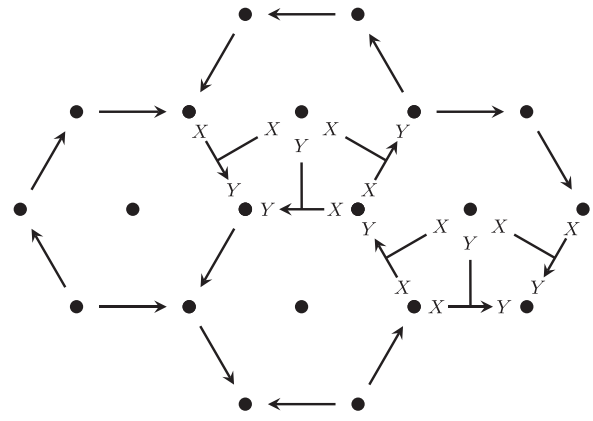

FIG. 8. Edge orientation, qubit placement, and edge operators for the hexagonal lattice mapping.

For every bottom edge of every face f, the edge operator acts on the face qubit of f with Y_f. The two edges adjacent to this bottom edge and also adjacent to f act on the face qubit of f with X_f. In this way all anticommutation relations are satisfied. Just as in the square lattice case, the vertex operators are Z operators on the vertex qubit. We illustrate this construction in Fig. 8.

Once again, the stabilizers of this mapping are cycles. However, in this case there are no trivial cycles, so there is a stabilizer generator for every face. This implies that the code space is the full fermionic space. One again, single fermion operators may be injected into the code at those vertices from which edges are either uniformly pointing towards or away. This mapping yields hopping and coulomb terms with Pauli weight at most 3. With M modes, this mapping uses fewer than 1.5M qubits.

Similar generalizations may be applied to other lattices.

APPENDIX C: PROOF OF CORRECTNESS OF SQUARE LATTICE FERMIONIC MAPPINGS

For the sake of completeness we include here a more explicit proof of our claims. The arguments presented here should be relatively familiar to those readers acquainted with fermionic mappings.

Definition 1. A mapping from some Hilbert space H_1 to another Hilbert space H_2 is an isometry[4] $J : H_1 \to H_2$, as defined in Ref. [13, Sec. 5].

Let $f_m = \mathbb{C}^m$ correspond to an m mode single fermion Hilbert space. The n fermion Fock space on m modes is defined as

$$\wedge^n f_m = \mathrm{span}\left(\frac{1}{n!}\sum_{\pi\in S_n}\mathrm{sgn}(\pi)\bigotimes_{i=1}^{n}\psi_{\pi(i)} : \psi_j \in f_m\right),$$

and the full fermionic Fock space of m modes is $F_m = \bigoplus_{n=0}^{m}(\wedge^n f_m)$. The dimension of F_m is 2^m. Let $F_m^E = \bigoplus_{n\in\mathrm{even}}^{m}(\wedge^n f_m)$ and $F_m^O = \bigoplus_{n\in\mathrm{odd}}^{m}(\wedge^n f_m)$. If m is even the dimension of F_m^E is 2^{m-1}.

In the following we denote with $L(S)$ to be the Linear operators on a space S, which form a C^*-algebra in the case where S is a complex Hilbert space.

Definition 2 (Fermionic Mapping). A fermionic mapping is an isometry $J : F_m \longrightarrow H$, where H is a qubit Hilbert space, i.e., J satisfies the property $J^\dagger J = \mathbb{I}_{F_m}$.

Proposition 2 ([13]). A $*$-isomorphism $\mu : L(H_1) \to L(H_2)$ induces an mapping $J : H_1 \longrightarrow H_2$ which is unique up to a global phase. An operator $X \in L(H_1)$ is represented via the map $\mu(X) = JXJ^\dagger$.

Proposition 3 ([13]). The algebra $L(F_m^E) \oplus L(F_m^O)$ is generated by the edge and vertex operators E_{ij} and V_i. The algebra $L(F_m)$ is generated by a single Majorana operator γ and the edge and vertex operators E_{ik} and V_i.

Theorem 2. A square $(L_1 \times L_2)$ lattice mapping with an even number of faces $n_F = (L_1 - 1)(L_2 - 1)$ (case I) is a fermionic mapping $J : F_m \to \mathcal{L}$, where $m = L_1L_2$ and $\mathcal{L} \subset (\mathbb{C}^2)^{m+n_F/2}$.

Proof. The mapping employs $m + n_F/2$ qubits. The number of nontrivial stabilizers is $n_F/2$. Let $\mathcal{L} \subset H = (\mathbb{C}^2)^{m+n_F/2}$ be the joint $+1$ eigenspace of these nontrivial stabilizers, then $\dim(\mathcal{L}) = 2^m = \dim(F_m)$.

If edge operators E_{jk} and vertex operators V_k satisfy the anticommutation relations

$$\{E_{jk}, V_j\} = 0, \quad \{E_{ij}, E_{jk}\} = 0, \tag{C1}$$

and for all $i \neq j \neq m \neq n$

$$[V_i, V_j] = 0, \quad [E_{ij}, V_m] = 0, \quad [E_{ij}, E_{mn}] = 0 \tag{C2}$$

and loop condition

$$i^{(|p|-1)}\prod_{i=1}^{(|p|-1)} E_{p_ip_{i+1}} = \mathbb{1}, \tag{C3}$$

then they generate the even fermionic algebra $L(F_m^E)$. To generate the entire fermionic algebra $L(F_m)$, we need an additional generator; for instance a single Majorana operator γ_i, which together with a vertex operator $V_i\gamma_i \propto c*_i$ generates the entire algebra $L(F_m)$.

By inspection the Pauli operators $\tilde{E}_{jk}$ and $\tilde{V}_k$ satisfy relations Eqs. (C1) and (C2). Furthermore, since the number of faces is even there are always exactly two corner faces of the lattice which are odd according to the checker-board labeling. Choose a corner vertex c, associated with an odd corner face, and define an encoded Majorana operator

$$\tilde{\gamma}_c = \begin{cases} X_c & \text{arrows pointing into corner, or} \\ Y_c & \text{otherwise.} \end{cases}$$

Then $\{\tilde{\gamma}_c, \tilde{E}_{cj}\} = \{\tilde{\gamma}_c, \tilde{V}_c\} = 0$.

By inspection we see that $\tilde{E}_{jk}$, $\tilde{V}_k$ and the additional Majorana $\tilde{\gamma}_c$ commute with the stabilizers of the mapping; as such, restriction to the joint $+1$ eigenspace $\mathcal{L}$ of the stabilizers—denoted $\cdot|_{\mathcal{L}}$—retains all their algebraic properties. Furthermore, the operators $\tilde{E}_{jk}|_{\mathcal{L}}$ satisfy Eq. (C3). Thus, by the same argument as in Ref. [13, Sec. 8], the identification

$$E_{jk} \longmapsto \tilde{E}_{jk}|_{\mathcal{L}} \quad V_k \longmapsto \tilde{V}_j|_{\mathcal{L}} \quad \gamma_c \longmapsto \tilde{\gamma}_c|_{\mathcal{L}}$$

extends to a $*$-homomorphism $\mu : L(F_m) \longrightarrow L(\mathcal{L})$. Since the CAR algebra is unique up to an isomorphism [22], and $\dim(\mathcal{L}) = \dim(F_m)$, the mapping is an isomorphism. The claim follows by Proposition 2. ■

Theorem 3. A square $(L_1 \times L_2)$ lattice mapping with an odd number of faces $n_F = (L_1 - 1)(L_2 - 1)$, and an extra even face (case II) describes an mapping $J : F_m^E \to \mathcal{L}$, where $m = L_1L_2$ and $\mathcal{L} \subset (\mathbb{C}^2)^{m+\lfloor n_F/2\rfloor}$.

Proof. The mapping employs $m + \lfloor n_F/2\rfloor$ qubits. The number of nontrivial stabilizers is $\lceil n_F/2\rceil$. Let $\mathcal{L} \subset (\mathbb{C}^2)^{m+\lfloor n_F/2\rfloor}$ be the $+1$ eigenspace of the nontrivial stabilizers, then $\dim(\mathcal{L}) = 2^{m+\lfloor n_F/2\rfloor-\lceil n_F/2\rceil} = 2^{(m-1)}$. Since n_F is odd, it must be the case that $L_1 - 1$ and $L_2 - 1$ are odd, and so m is even. Thus, $\dim(F_m^E) = 2^{m-1} = \dim(\mathcal{L})$.

$L(F_m^E) \oplus L(F_m^O)$ is generated by E_{ij} and V_i. However, under the algebraic constraint that $\prod_i V_i = \mathbb{I}$, the algebra only generates $L(F_m^E)$. Thus, we have a mapping $\mu : L(F_m^E) \to L(\mathcal{L})$ by $\mu(E_{ij}) = \tilde{E}_{ij}|_{\mathcal{L}}$ and $\mu(V_i) = \tilde{V}_i|_{\mathcal{L}}$. By a similar argument to the previous theorem, μ is a *-isomorphism, and therefore specifies an mapping $J : F_m^E \to \mathcal{L}$. ■

[4] $J^\dagger J = \mathbb{I}_{H_1}$ and $JJ^\dagger = \mathrm{Proj}[\mathrm{Image}(J)]$.

Theorem 4. A square $(L_1 \times L_2)$ lattice mapping with an odd number of faces $n_F = (L_1 - 1)(L_2 - 1)$, and an extra odd face (case III), is a fermionic mapping $J : \mathbb{C}^2 \otimes F_m \to \mathcal{L}$, where $m = L_1 L_2$ and $\mathcal{L} \subset (\mathbb{C}^2)^{m+\lceil n_F/2 \rceil}$.

Proof. The mapping employs $m + \lceil n_F/2 \rceil$ qubits. The number of nontrivial stabilizers is $\lfloor n_F/2 \rfloor$. Let $\mathcal{L} \subset (\mathbb{C}^2)^{m+\lceil n_F/2 \rceil}$ be the $+1$ eigenspace of the nontrivial stabilizers, then $\dim(\mathcal{L}) = 2^{(m+1)} = \dim(\mathbb{C}^2 \otimes F_m^E)$.

There are four corner faces of the lattice which are odd according to the checker-board labeling. One may choose a corner vertex c and define an encoded operator acting trivially on the logical qubit, and as a Majorana on the logical fermionic space: $\tilde{\mathbb{I}} \otimes \tilde{\gamma}_c = X_c$ or Y_c depending on if the arrows point into or, respectively, away from that corner. The other three corners, which we label c_x, c_y, c_z, may then be defined as logical Pauli operators combined with logical hole operators:

$$\tilde{X} \otimes \tilde{h}_{c_x} = X_{c_x} \text{ or } Y_{c_x},$$
$$\tilde{Y} \otimes \tilde{h}_{c_y} = X_{c_y} \text{ or } Y_{c_y},$$
$$\tilde{Z} \otimes \tilde{h}_{c_z} = X_{c_z} \text{ or } Y_{c_z}.$$

Here the choice of which corners to associate with which logical Paulis is a matter of convention, and the choice of X or Y will again depend on if the arrows point into or, respectively, away from that corner.

By Proposition 3, the operators $\mathbb{I} \otimes \gamma_j$, $X \otimes h_j$ and $Y \otimes h_j$, along with the edge and vertex operators, generate $L(\mathbb{C}^2 \otimes F_m)$. Define the mapping $\mu : L(\mathbb{C}^2 \otimes F_m) \to L(\mathcal{L})$ by $\mu(\mathbb{I} \otimes \gamma_c) = \tilde{I} \otimes \tilde{\gamma}_c|_{\mathcal{L}}$ etc. By a similar argument to the previous theorems, μ is a *-isomorphism, and therefore specifies an mapping $J : \mathbb{C}^2 \otimes F_m \to \mathcal{L}$. ∎

APPENDIX D: DERIVATION OF FERMIONIC PHASE NOISE

To illustrate the fact that phase noise can be considered natural fermionic noise, we present a derivation of fermionic phase noise for a natural fermionic system. Here we consider a fermionic lattice model coupled to a bosonic system, for example phonons on the lattice. The interaction is mediated through the transfer of momentum; a coupling known as Fröhlich Hamiltonian [23,24], which reads

$$H := \sum_{\mathbf{k},\sigma} \sum_{\mathbf{q}} g_{\mathbf{q}} a^\dagger_{\mathbf{k}+\mathbf{q},\sigma} a_{\mathbf{k},\sigma} (b_{\mathbf{q}} + b^\dagger_{-\mathbf{q}}). \tag{D1}$$

Assume for simplicity a momentum-independent coupling $g_q = g := 1$.[5] A Fourier transform of the fermionic and bosonic operators yields

$$H = \sum_{\mathbf{x}} N_{\mathbf{x}} (b_{\mathbf{x}} + b^\dagger_{\mathbf{x}}), \tag{D2}$$

where $N_{\mathbf{x}} = \sum_\sigma N_{\mathbf{x},\sigma}$ and $N_{\mathbf{x},\sigma}$ is the fermionic number operator for spin $\sigma \in \{\uparrow, \downarrow\}$ on site $\mathbf{x}$. Given an interaction strength γ, the interaction unitary is $U := \mathrm{e}^{-\mathrm{i}\gamma H}$.

The effective channel on the spin-up fermionic system is then given by

$$\Lambda(\rho_{\mathcal{F}\uparrow}) = \mathrm{Tr}_{\mathcal{B},\mathcal{F}\downarrow}[U(\rho_{\mathcal{F}\uparrow} \otimes \bar{I}_{\mathcal{F}\downarrow} \otimes \rho_{\mathcal{B}})U^\dagger]. \tag{D3}$$

$\bar{I}_{\mathcal{F}\downarrow}$ is the maximally mixed state on the spin-down fermionic system, and $\rho_{\mathcal{B}}$ is a finite temperature Gibbs state with inverse temperature β on the bosonic system, which we assumed to be in a completely thermalized bath configuration. Expanding in the Fock basis $|\mathbf{m}\rangle$ of $\mathcal{B}$ and $|\mathbf{n}\rangle$ of $\mathcal{F}_\downarrow$ we retrieve

$$\Lambda(\rho_{\mathcal{F}\uparrow}) = \frac{1}{d_{\mathcal{F}\downarrow}} \sum_{\mathbf{nn}'} \sum_{\mathbf{mm}'} \frac{e^{-\beta|\mathbf{m}'|}}{Z} U_{\mathbf{nm};\mathbf{n}'\mathbf{m}'} \rho_{\mathcal{F}\uparrow} U^\dagger_{\mathbf{n}'\mathbf{m}';\mathbf{nm}}, \tag{D4}$$

where $d_{\mathcal{F}\downarrow}$ denotes the dimension of the fermionic spin down subsystem and $U_{\mathbf{nm};\mathbf{n}'\mathbf{m}'} = \langle \mathbf{n}, \mathbf{m}|U|\mathbf{n}', \mathbf{m}'\rangle$ is an operator acting on the fermionic spin up sector. We note that for a bosonic Fock state $\langle \mathbf{m}|H|\mathbf{m}\rangle = 0$, such that a second order expansion in γ yields

$$\begin{aligned}\Lambda(\rho_{\mathcal{F}\uparrow}) = {} & \mathrm{O}(\gamma^3) + \rho_{\mathcal{F}\uparrow} \\ & + \frac{\gamma^2}{d_{\mathcal{F}\downarrow}} \sum_{\substack{\mathbf{nn}' \\ \mathbf{mm}'}} \frac{e^{-\beta|\mathbf{m}'|}}{Z} H_{\mathbf{nm};\mathbf{n}'\mathbf{m}'} \rho_{\mathcal{F}\uparrow} H_{\mathbf{n}'\mathbf{m}';\mathbf{nm}} \\ & - \frac{\gamma^2}{2d_{\mathcal{F}\downarrow}} \sum_{\mathbf{nm}} \frac{e^{-\beta|\mathbf{m}|}}{Z} ([H^2]_{\mathbf{nm};\mathbf{nm}} \rho_{\mathcal{F}\uparrow} \\ & + \rho_{\mathcal{F}\uparrow} [H^2]_{\mathbf{nm};\mathbf{nm}}).\end{aligned} \tag{D5}$$

Expanding H and isolating bosonic terms:

$$\begin{aligned}\Lambda(\rho_{\mathcal{F}\uparrow}) = {} & \mathrm{O}(\gamma^3) + \rho_{\mathcal{F}\uparrow} \\ & + \frac{\gamma^2}{d_{\mathcal{F}\downarrow}} \sum_{\substack{\mathbf{nn}' \\ \mathbf{xx}'}} \Gamma_{\mathbf{xx}'}(\beta) \langle \mathbf{n}|N_{\mathbf{x}}|\mathbf{n}'\rangle \rho_{\mathcal{F}\uparrow} \langle \mathbf{n}'|N_{\mathbf{x}'}|\mathbf{n}\rangle \\ & - \frac{\gamma^2}{2d_{\mathcal{F}\downarrow}} \sum_{\substack{\mathbf{n} \\ \mathbf{xx}'}} \Omega_{\mathbf{xx}'}(\beta) (\langle \mathbf{n}|N_{\mathbf{x}} N_{\mathbf{x}'}|\mathbf{n}\rangle \rho_{\mathcal{F}\uparrow} \\ & + \rho_{\mathcal{F}\uparrow} \langle \mathbf{n}|N_{\mathbf{x}} N_{\mathbf{x}'}|\mathbf{n}\rangle t),\end{aligned} \tag{D6}$$

where

$$\Gamma_{\mathbf{xx}'}(\beta) = \sum_{\mathbf{mm}'} \frac{e^{-\beta|\mathbf{m}'|}}{Z} \langle \mathbf{m}|(b_{\mathbf{x}} + b^\dagger_{\mathbf{x}})|\mathbf{m}'\rangle \langle \mathbf{m}'|(b_{\mathbf{x}'} + b^\dagger_{\mathbf{x}'})|\mathbf{m}\rangle$$

and

$$\begin{aligned}\Omega_{\mathbf{xx}'}(\beta) &:= \sum_{\mathbf{m}} \langle \mathbf{m}|(b_{\mathbf{x}} + b^\dagger_{\mathbf{x}})(b_{\mathbf{x}'} + b^\dagger_{\mathbf{x}'})|\mathbf{m}\rangle \frac{e^{-\beta|\mathbf{m}|}}{Z} \qquad \text{(D7)} \\ &= \sum_{\mathbf{mm}'} \langle \mathbf{m}'|(b_{\mathbf{x}'} + b^\dagger_{\mathbf{x}'})|\mathbf{m}\rangle \langle \mathbf{m}|(b_{\mathbf{x}} + b^\dagger_{\mathbf{x}})|\mathbf{m}'\rangle \frac{e^{-\beta|\mathbf{m}|}}{Z} \\ &= \Gamma_{\mathbf{xx}'}(\beta). \qquad \text{(D8)}\end{aligned}$$

[5] A more sophisticated and realistic analysis could be performed for a momentum-dependent coupling but is beyond the scope of this paper.

Noting that $\Gamma_{\mathbf{x}\mathbf{x}'}(\beta) = \delta_{\mathbf{x}\mathbf{x}'}\Gamma_{\mathbf{x}\mathbf{x}}(\beta) = \Gamma(\beta)\delta_{\mathbf{x}\mathbf{x}'}$, we get

$$\Lambda(\rho_{\mathcal{F}\uparrow}) = \mathrm{O}(\gamma^3) + \rho_{\mathcal{F}\uparrow} + \frac{\gamma^2}{d_{\mathcal{F}\downarrow}}\Gamma(\beta)\sum_{\substack{\mathbf{n}\mathbf{n}'\\\mathbf{x}}}\langle\mathbf{n}|N_{\mathbf{x}}|\mathbf{n}'\rangle\rho_{\mathcal{F}\uparrow}\langle\mathbf{n}'|N_{\mathbf{x}}|\mathbf{n}\rangle - \frac{\gamma^2}{2d_{\mathcal{F}\downarrow}}\Gamma(\beta)\sum_{\mathbf{n}\mathbf{x}}\langle\mathbf{n}|N_{\mathbf{x}}^2|\mathbf{n}\rangle\rho_{\mathcal{F}\uparrow} + \rho_{\mathcal{F}\uparrow}\langle\mathbf{n}|N_{\mathbf{x}}^2|\mathbf{n}\rangle. \tag{D9}$$

Given that we only work in a fermionic Fock basis $|\mathbf{n}\rangle$ on the spin-down sector, we have

$$\langle\mathbf{n}|N_{\mathbf{x}}|\mathbf{n}'\rangle = (N_{\mathbf{x},\uparrow} + [\mathbf{n}]_{\mathbf{x}})\delta_{\mathbf{n},\mathbf{n}'}, \tag{D10}$$

where $[\mathbf{n}]_{\mathbf{x}}$ is the $\mathbf{x}$th element of the vector $\mathbf{n}$. We therefore retrieve

$$\begin{aligned}\Lambda(\rho_{\mathcal{F}\uparrow}) = \mathrm{O}(\gamma^3) + \rho_{\mathcal{F}\uparrow} + \frac{\gamma^2}{d_{\mathcal{F}\downarrow}}\Gamma(\beta)\sum_{\mathbf{n}\mathbf{x}}(N_{\mathbf{x},\uparrow} + [\mathbf{n}]_{\mathbf{x}})\rho_{\mathcal{F}\uparrow}(N_{\mathbf{x},\uparrow} + [\mathbf{n}]_{\mathbf{x}})\\ - \frac{\gamma^2}{2d_{\mathcal{F}\downarrow}}\Gamma(\beta)\sum_{\mathbf{n}\mathbf{x}}(N_{\mathbf{x},\uparrow} + [\mathbf{n}]_{\mathbf{x}})^2\rho_{\mathcal{F}\uparrow} + \rho_{\mathcal{F}\uparrow}(N_{\mathbf{x},\uparrow} + [\mathbf{n}]_{\mathbf{x}})^2.\end{aligned} \tag{D11}$$

Noting that $\sum_{\mathbf{n}}[\mathbf{n}]_{\mathbf{x}} = d_{\mathcal{F}\downarrow}/2$ (as we sum over all possible configurations; and a mode is occupied half of the time) and $\sum_{\mathbf{n}}(N_{\mathbf{x}\uparrow} + [\mathbf{n}]_{\mathbf{x}})^2 = d_F(2N_{\mathbf{x}\uparrow} + 1/2)$ and expanding terms yields

$$\begin{aligned}\Lambda(\rho_{\mathcal{F}\uparrow}) = \mathrm{O}(\gamma^3) + \rho_{\mathcal{F}\uparrow} + \gamma^2\Gamma(\beta)\sum_{\mathbf{x}}\left(N_{\mathbf{x},\uparrow}\rho_{\mathcal{F}\uparrow}N_{\mathbf{x},\uparrow} + \frac{1}{2}(N_{\mathbf{x},\uparrow}\rho_{\mathcal{F}\uparrow} + \rho_{\mathcal{F}\uparrow}N_{\mathbf{x},\uparrow}) + \frac{1}{2}\rho_{\mathcal{F}\uparrow}\right)\\ - \frac{\gamma^2\Gamma(\beta)}{2}\sum_{\mathbf{x}}(2N_{\mathbf{x}\uparrow} + 1/2)\rho_{\mathcal{F}\uparrow} + \rho_{\mathcal{F}\uparrow}(2N_{\mathbf{x}\uparrow} + 1/2)\end{aligned} \tag{D12}$$

$$= \mathrm{O}(\gamma^3) + \rho_{\mathcal{F}\uparrow} + \gamma^2\Gamma(\beta)\sum_{\mathbf{x}}\left(N_{\mathbf{x},\uparrow}\rho_{\mathcal{F}\uparrow}N_{\mathbf{x},\uparrow} - \frac{1}{2}(N_{\mathbf{x},\uparrow}\rho_{\mathcal{F}\uparrow} + \rho_{\mathcal{F}\uparrow}N_{\mathbf{x},\uparrow})\right). \tag{D13}$$

Substituting the phase operator $\phi_{\mathbf{x}\uparrow} := (1 - 2N_{\mathbf{x}\uparrow})$ yields

$$\Lambda(\rho_{\mathcal{F}\uparrow}) = \left(1 - \frac{\gamma^2\Gamma(\beta)M}{4}\right)\rho_{\mathcal{F}\uparrow} + \frac{\gamma^2\Gamma(\beta)M}{4}\sum_{\mathbf{x}}\frac{1}{M}\phi_{\mathbf{x},\uparrow}\rho_{\mathcal{F}\uparrow}\phi_{\mathbf{x},\uparrow}, \tag{D14}$$

where M is the number of modes.

[1] G. C. Wick, A. S. Wightman, and E. P. Wigner, The intrinsic parity of elementary particles, Phys. Rev. **88**, 101 (1952).

[2] M. Levin and X.-G. Wen, Fermions, strings, and gauge fields in lattice spin models, Phys. Rev. B **67**, 245316 (2003).

[3] E. P. Wigner and P. Jordan, Über das Paulische Äquivalenzverbot, Z. Phys. **47**, 631 (1928).

[4] S. Lloyd, Universal quantum simulators, Science **273**, 1073 (1996).

[5] D. S. Abrams and S. Lloyd, Simulation of Many-Body Fermi Systems on a Universal Quantum Computer, Phys. Rev. Lett. **79**, 2586 (1997).

[6] A. M. Childs, Y. Su, M. C. Tran, N. Wiebe, and S. Zhu, Theory of Trotter Error with Commutator Scaling, Phys. Rev. X **11**, 011020 (2021).

[7] V. Havlíček, M. Troyer, and J. D. Whitfield, Operator locality in the quantum simulation of fermionic models, Phys. Rev. A **95**, 032332 (2017).

[8] L. Clinton, J. Bausch, and T. S. Cubitt, Hamiltonian simulation algorithms for near-term quantum hardware, arXiv:2003.06886.

[9] C. Cade, L. Mineh, A. Montanaro, and S. Stanisic, Strategies for solving the Fermi-Hubbard model on near-term quantum computers, Phys. Rev. B **102**, 235122 (2020).

[10] F. Verstraete and J. I. Cirac, Mapping local Hamiltonians of fermions to local Hamiltonians of spins, J. Stat. Mech.: Theory Exp. (2005) P09012.

[11] J. D. Whitfield, V. Havlíček, and M. Troyer, Local spin operators for fermion simulations, Phys. Rev. A **94**, 030301(R) (2016).

[12] M. Steudtner and S. Wehner, Quantum codes for quantum simulation of fermions on a square lattice of qubits, Phys. Rev. A **99**, 022308 (2019).

[13] S. B Bravyi and A. Yu Kitaev, Fermionic quantum computation, Ann. Phys. **298**, 210 (2002).

[14] K. Setia, S. Bravyi, A. Mezzacapo, and J. D. Whitfield, Superfast encodings for fermionic quantum simulation, Phys. Rev. Res. **1**, 033033 (2019).

[15] Z. Jiang, J. McClean, R. Babbush, and H. Neven, Majorana Loop Stabilizer Codes for Error Mitigation in Fermionic Quantum Simulations, Phys. Rev. Appl. **12**, 064041 (2019).

[16] A. Yu. Kitaev, Fault-tolerant quantum computation by anyons, Ann. Phys. **303**, 2 (2003).

[17] L. Savary and L. Balents, Quantum spin liquids: A review, Rep. Prog. Phys. **80**, 016502 (2016).

[18] T. S. Cubitt, A. Montanaro, and S. Piddock, Universal quantum Hamiltonians, Proc. Natl. Acad. Sci. USA **115**, 9497 (2018).

[19] L. Fedichkin and A. Fedorov, Decoherence rate of semiconductor charge qubit coupled to acoustic phonon reservoir, Phys. Rev. A **69**, 032311 (2004).

[20] H. Bruus and K. Flensberg, *Many-Body Quantum Theory in Condensed Matter Physics: An Introduction* (Oxford University Press, Oxford, UK, 2004).

[21] A. A. Melnikov and L. E. Fedichkin, Quantum walks of interacting fermions on a cycle graph, Sci. Rep. UK **6**, 34226 (2016).

[22] J. T. Ottesen, *Infinite Dimensional Groups and Algebras in Quantum Physics* (Springer, Berlin, 1995), pp. 13–59.

[23] H. Fröhlich, Electrons in lattice fields, Adv. Phys. **3**, 325 (1954).

[24] E. Pavarini, E. Koch, R. Martin, and R. Scalettar, *The physics of correlated insulators, metals, and superconductors*, FZJ-2017-06396 (Theoretische Nanoelektronik, Jülich, 2017).